

# Measurements of $^{17}\text{F}$ scattering by $^{208}\text{Pb}$ with a new type of large solid angle detector array

M. Romoli,\* E. Vardaci, M. Di Pietro, A. De Francesco, A. De Rosa,

G. Inghima, M. La Commara, B. Martin, D. Pierroutsakou, and M. Sandoli

*Department of Physical Science and INFN, Complesso Universitario di Monte S. Angelo, via Cinthia, I-80125 Napoli, Italy*

M. Mazzocco, T. Glodariu,† P. Scopel, and C. Signorini

*Department of Physics and INFN, via Marzolo 8, I-35131 Padova, Italy*

R. Bonetti and A. Guglielmetti

*Institute of General Physics and INFN, Milano, via Celoria 16, I-20133, Milano, Italy*

F. Soramel

*Department of Physics and INFN, Udine, via delle Scienze 208, I-33100, Udine, Italy*

L. Stroe†

*INFN Laboratori Nazionali di Legnaro, viale dell'Università 2, I-35020 Legnaro (Padova), Italy*

J. Greene, A. Heinz, D. Henderson, C. L. Jiang, E. F. Moore, R. C. Pardo, K. E. Rehm, and A. Wuosmaa

*Physics Division, Argonne National Laboratory, Argonne, Illinois 60439, USA*

J. F. Liang

*Physics Division, Oak Ridge National Laboratory, Oak Ridge, Tennessee 37831, USA*

(Dated: February 12, 2004)

A new pixel-structure detector array with a large solid angle coverage has been used for the first time to study the elastic scattering of exotic  $^{17}\text{F}$  nuclei from a  $^{208}\text{Pb}$  target at 90.4 MeV. The experimental data have been analyzed in the framework of the optical model potential and the real and imaginary strong absorption radii have been evaluated. These quantities have been compared with those obtained for the system  $^{19}\text{F} + ^{208}\text{Pb}$  at the same energy in the center of mass frame. The  $^{17}\text{F} + ^{208}\text{Pb}$  reaction cross section is more similar to those of the systems  $^{16,17}\text{O} + ^{208}\text{Pb}$  rather than to the one of the system  $^{19}\text{F} + ^{208}\text{Pb}$  at similar energies: this indicates that in the energy range around the Coulomb barrier the breakup channel is still weak. The exclusive breakup cross section  $^{17}\text{F} \rightarrow ^{16}\text{O} + p$  has been measured for the first time at energy below the Coulomb barrier.

PACS numbers: 25.70.Bc, 25.70.Mn, 24.10.Eq

## I. INTRODUCTION

Over the last decade, there has been a growing interest in the study of the nuclear reactions induced by light weakly bound Radioactive Ion Beams (RIBs). Because of halo/skin structure and the small binding energy of the last nucleon(s), these nuclei are expected to behave differently from stable, well-bound nuclei, in reactions (elastic scattering, fusion, breakup, transfer) taking place at Coulomb barrier energies.

On a simple ground, loosely-bound nuclei are expected to have a larger flux into non-elastic channels than stable nuclei. This behaviour was predicted for example for the  $^{11}\text{Be} + ^{197}\text{Au}$  [1] system and, up to now, several experiments have been performed to study the scattering

of loosely-bound nuclei from heavy targets:  $^6\text{He} + ^{209}\text{Bi}$  [2] ( $S_{2n} = 0.945$  MeV),  $^9\text{Be} + ^{209}\text{Bi}$  [3] ( $S_n = 1.573$  MeV) and  $^6\text{Li} + ^{208}\text{Pb}$  [4, 5] ( $S_d = 1.475$  MeV). For the first system a very large reaction cross section was deduced, while in the others both real and imaginary potentials showed “threshold anomaly” effects around the Coulomb barrier. In addition, in all the systems ( $^6\text{He}$  [2],  $^9\text{Be}$  [6] and  $^6\text{Li}$  [7]) strong breakup cross sections have been measured.

Our interests for the physics exploited by RIBs have motivated the study of the  $^{17}\text{F}$  elastic scattering from a  $^{208}\text{Pb}$  target around the Coulomb barrier. The study of this nucleus is quite interesting for three reasons: (i) its binding energy is 601 keV, (ii) it has only one bound state below the breakup threshold and (iii) its first excited state has a halo structure [8, 9].

For the experiment we used the  $^{17}\text{F}$  beam delivered by the ATLAS facility at the ANL Physics Division [10]. Such a beam belongs to the first generation of RIBs, which are produced with very low intensities (at least a factor  $10^4$  lower than stable beams) and poor energy

---

\*Electronic address: romoli@na.infn.it

†On leave from National Institute for Physics and Nuclear Engineering, 76900 Magurele-Ilf, Romania

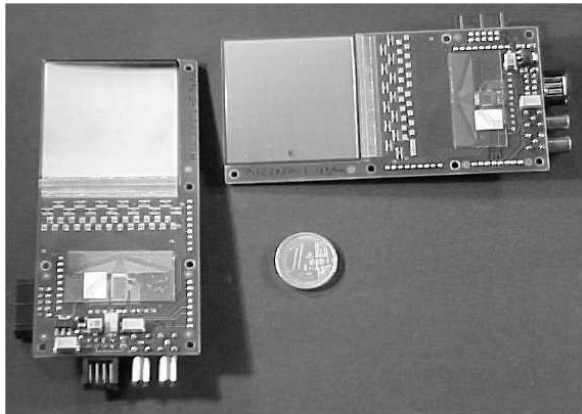


FIG. 1: Photo of two detectors of an EXODET telescope before their assembling.

resolution. For these reasons the study of RIBs exotic features requires the design of detector arrays with large solid angle coverage and an energy and position resolution good enough to guarantee the complete kinematic reconstruction of the events.

These requirements have brought us to design and develop a new detector array named EXODET (EXOtIC DETector) briefly presented in the next section.

The present paper is organized as follows. In Sec. II we will introduce the new detector array EXODET; Section III will briefly describe the  $^{17}\text{F}$  secondary beam production and the experimental procedure adopted in the data analysis both for elastic scattering and exclusive breakup cross sections. Section IV will present the performed optical model analysis of the experimental data and the discussion about the comparison with similar systems in the same energy range. In Sec. V conclusive comments will be drawn.

## II. DETECTOR ARRAY DESCRIPTION

The EXODET array consists of 16 solid state silicon detectors arranged in 8 two-stage telescopes to allow the Z identification of the particles passing through the first layer, by means of the usual  $\Delta E$ -E technique. The thicknesses of the first and the second layer are,  $60\ \mu\text{m}$  and  $500\ \mu\text{m}$ , respectively. The telescopes are placed around the target, in the forward and backward direction, and can cover a total solid angle up to 70% of  $4\pi$  sr.

Each detector has an active area of  $50 \times 50\ \text{mm}^2$  and is segmented, on the front side, in 100 strips with a pitch size of  $0.5\ \text{mm}$  and a separation of  $50\ \mu\text{m}$ . The backplane is a unique plaque. The strips of the  $\Delta E$  layer are mounted orthogonally to the beam direction and perpendicularly to the strips of the E layer. In this way it is possible to determine the position of the particles passing through the  $\Delta E$  detector with an accuracy of  $0.5\ \text{mm} \times 0.5\ \text{mm}$ .

The whole array readout system has to consider 16

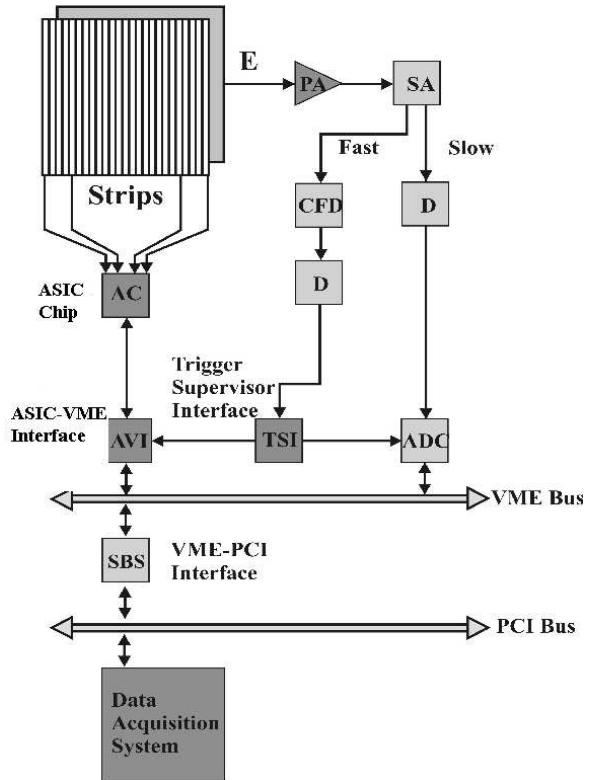


FIG. 2: Schematic of the electronic circuit for one of the EXODET detectors.

channels for the processing of the energy signals from the backplane of the detectors, and 1600 channels for the position information gathered from the segmented sides. For the energy channels standard electronic chain has been used, whereas the position information was obtained through the use of an ASIC chipset. Such a device, originally developed for high-energy particle physics experiments [11], was found to be suitable with an appropriate design of the readout electronics. A proper signal amplitude attenuator was built in order to reach the required dynamic range together with a pitch size adapter for connecting the detector strips to the input pads of the chip. The chip and the related electronics are placed on a support board near the detector, to ensure the maximum noise reduction. Fig. 1 shows a photo of both  $\Delta E$  and E detector boards with the readout chips.

Fig. 2 shows a schematic diagram of the electronic readout chain. The board containing the silicon detector and the chip is interfaced to the VME bus through the AVI (ASIC to VME Interface) board. There is one AVI board per chip. The TSI board (Trigger Supervisor Interface) is the trigger supervisor of the whole front-end. When the acquisition is running and the TSI board asserts a valid trigger signal, the AVI sends the trigger command to the chip and makes available to the VME bus the data stream coming from the chip. The TSI board uses a logical combination (OR/AND) of all of the input channels to assert a valid trigger.

Each chip gives as output a data stream with the chip identification number, the trigger number and, for each strip hit, the identification number, the signal ToT (Time Over Threshold) and the JT (Jitter Time). The JT gives information about the time interval between the strip signal and the trigger assertion, while the ToT is roughly proportional to the energy released by the particle in the strip. This information is very useful to disentangle an event when two particles with different energy ranges hit two strips of the same detector.

The VME bus is, in the present set-up, connected to a PC via a commercial VME-PCI bridge. All of the processes concerning the data acquisition (module setup, run control, data readout, storing and histogramming) run on a single PC using Linux as the operating system. The data analysis has been performed with the package VISM.

### III. EXPERIMENT

#### A. $^{17}\text{F}$ secondary beam

The  $^{17}\text{F}$  exotic beam is produced at the Argonne National Laboratory (ANL) through the inverse reaction  $p(^{17}\text{O}, ^{17}\text{F})n$  [10] with an intensity of about  $10^6$  pps. A high intensity  $^{17}\text{O}$  primary beam, delivered by the ATLAS superconducting linear accelerator, impinges on a gas cell, filled with hydrogen. Because of the inverse kinematics of the reaction, the  $^{17}\text{F}$  ions are emitted in a narrow cone ( $\sim 2\text{-}4^\circ$ ) in the forward direction. During the experiment the energy of the outgoing  $^{17}\text{F}$  beam, measured with an Enge split pole magnetic spectrometer, was 90.4 MeV, with a FWHM of 1.4 MeV (corresponding to a resolution of about 1.5%). The beam diameter was  $\sim 5$  mm at the target position. The main contaminant in the secondary beam was  $^{17}\text{O}$ , with the same magnetic rigidity as  $^{17}\text{F}$ , but with an energy  $\sim (8/9)^2 \cdot E(^{17}\text{F})$ . From Fig. 3a one can clearly see that the intensities of the two beams were comparable.

#### B. Experimental set-up

In this first experiment only a section of the whole EXODET array was used. A two-stage telescope was placed in the backward direction to cover the polar angles ranging from  $98^\circ$  up to  $154^\circ$ ; another one was placed at forward angles to cover the polar angles from  $26^\circ$  to  $82^\circ$ . The telescope at the forward angles was used for data normalization since the cross section at forward angles is expected to be purely Rutherford in the energy range of the experiment. The target was a self supporting 1 mg/cm<sup>2</sup> thick  $^{208}\text{Pb}$  foil.

During the experiment, the data acquisition system was triggered by the logical “OR” of all the energy signals. The collected data were: the energy signals coming from the not-segmented sides of the  $\Delta E$  and E detectors,

and the positional information processed by the ASIC chip: hit strip number, Jitter Time (JT) and Time Over Threshold (ToT).

The JT represents the time interval, measured in units of clock cycles, between the assertion of the trigger and the arrival of the particle signal. The best time resolution achievable with the chip used was 67 ns.

The ToT is the time, measured in units of clock cycles, spent by any signal, after its amplification and shaping, over an externally settable threshold in the ASIC chip. Since only 4 bits are available for the ToT counter, this spectrum is distributed only over 16 channels. Due to the non-linear correspondence between the ToT and the signal amplitude, the ToT only gives a rough information about the energy lost by a particle in the strip.

Regardless of the limited time and energy resolution, the ToT range is sufficient to separate two particles with different energy domains hitting two different strips of the same  $\Delta E$  detector. This feature is particularly helpful for the selection of breakup events  $^{17}\text{F} \rightarrow ^{16}\text{O} + p$ . In fact, the  $^{17}\text{F}$  breakup channel produces two particles, a proton and a  $^{16}\text{O}$  ion, which can hit the same  $\Delta E$  detector of a telescope. Their expected energies are such that the  $^{16}\text{O}$  ion is stopped in the  $\Delta E$  stage and the proton in the second stage. From the kinematics of the process the proton will deposit in one strip a much smaller energy signal than the  $^{16}\text{O}$  would deposit in another strip. Consequently, using the ToT information, it is possible to distinguish which of the two strips was hit by the proton and which one was hit by the  $^{16}\text{O}$  ion.

From the data we determined the  $^{17}\text{F}$  scattering angular distribution at backward angles and we performed a first direct measurement of the  $^{17}\text{F} \rightarrow ^{16}\text{O} + p$  ( $S_p = 0.601$  MeV) exclusive breakup cross section at energies below the Coulomb barrier, with the only limitation of the statistical accuracy.

#### C. Experimental results

Fig. 3a shows a typical  $\Delta E$  spectrum collected from the backward telescope. It is possible to distinguish three broad structures. On the high energy side there are two wide bumps: the one at higher energy arises from  $^{17}\text{F}$  scattering and the other, at lower energy, comes from the elastic scattering of the  $^{17}\text{O}$  contaminant, whose energy is around  $(8/9)^2 \cdot E(^{17}\text{F})$ . Their broad structures are mainly due to the large solid angle covered by the detector and to the energy lost in the target. The overall energy resolution of  $\sim 18\%$  (see Fig. 3b) essentially originates from the large kinematic spread ( $\theta = 98^\circ$  to  $\theta = 154^\circ$ ). However, an energy resolution of 3-4% is achieved by selecting a limited number of strips. In Fig. 3a at low energies, one can see a third peak originating from light particles as explained in the following section.

Considering the JT and the ToT spectra of all the  $\Delta E$  events, it is possible to disentangle the components of the spectrum in Fig. 3a. Fig. 4a shows the JT spectrum of

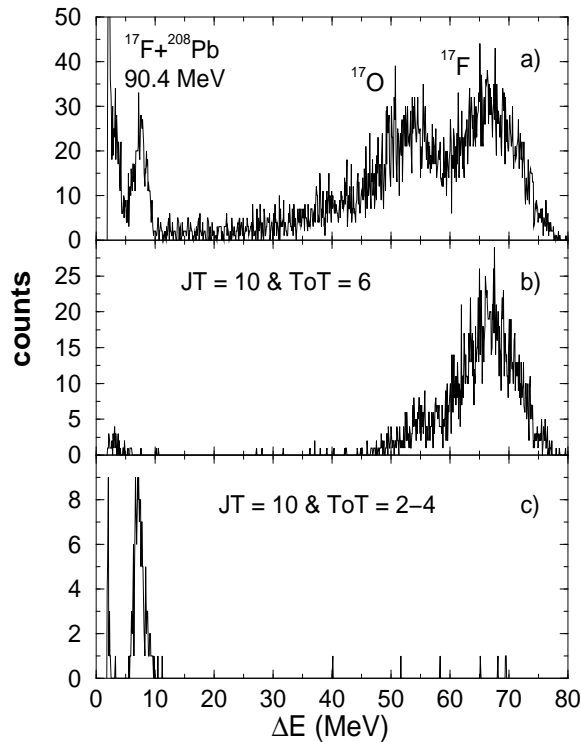


FIG. 3: a)  $\Delta E$  spectrum collected from the backward detector of the EXODET apparatus; b)  $\Delta E$  spectrum gated by JT = 10 and ToT = 6; c)  $\Delta E$  spectrum gated by JT = 10 and ToT ranging from 2 to 4. See text for more details on JT and ToT.

the events hitting the  $\Delta E$  detector. The presence of a very sharp peak indicates the time correlation of all the recorded events. This is useful to avoid spurious and/or uncorrelated events. For this reason only the events with JT around 10 will be considered in the following analysis.

Fig. 4 also shows two ToT spectra of  $\Delta E$  events: the upper one (b) for the scattered  $^{17}\text{F}$  ions energy range and the lower one (c) for the light particle energy range. We clearly see that the  $^{17}\text{F}$  scattering events have a ToT sharply peaked around 400 ns ( $6 \times 67$  ns), whereas, for light particles, this parameter is smaller than 266 ns ( $4 \times 67$  ns).

Fig. 3b shows the  $\Delta E$  spectrum gated by the 10<sup>th</sup> channel of the JT spectrum and the 6<sup>th</sup> channel of the ToT: practically only the  $^{17}\text{F}$  elastic peak survives these gates. Fig. 3c shows the same  $\Delta E$  spectrum, but gated by the lower ToT channels (from 2 to 4) and the 10<sup>th</sup> JT channel. In this case only low energy events populate the resulting spectrum. This is a clear indication of the capabilities given by the analysis of the information processed by the ASIC chip.

### 1. $^{17}\text{F}$ scattering event analysis

For the analysis of the  $^{17}\text{F}$  scattering from a  $^{208}\text{Pb}$  target the events in the Fluorine peak and with JT =

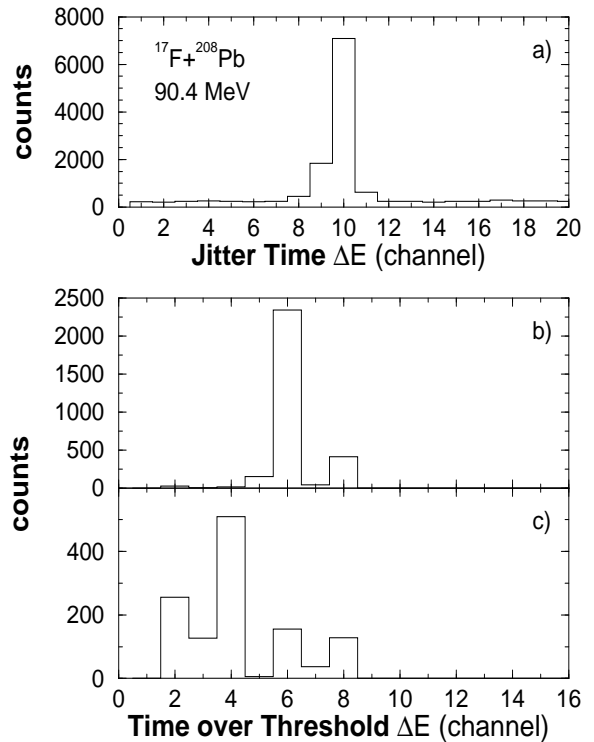


FIG. 4: a) Jitter Time (JT) spectrum of the backward  $\Delta E$  detector. Lower panel: Time over Threshold (ToT) spectra of the events collected by the  $\Delta E$  detector at backward angles with: b) JT = 10 and energy loss greater than 59 MeV (corresponding to the  $^{17}\text{F}$  peak), c) JT = 10 and energy loss smaller than 10 MeV (light particle range).

10 and ToT = 6 were considered. At 90.4 MeV beam energy all  $^{17}\text{F}$  nuclei were stopped in the  $\Delta E$  detector, making a  $\Delta E$ -E pixel analysis impossible. Our experimental energy resolution did not allow to separate the contributions coming from the first excited states both in  $^{17}\text{F}$  (at 0.4953 keV) and in  $^{208}\text{Pb}$  (at 2.614 MeV). However, from DWBA calculations, as we will see in the discussion, these contributions were predicted to be very small in comparison with the pure elastic cross section.

Due to the geometry of the detectors, each strip covers a wide range of polar angles  $\theta$ . For this reason, a Monte-Carlo simulation of the detector geometry was undertaken in order to calculate the polar angles  $\theta$ , the solid angles  $\Delta\Omega_s$  subtended by each  $\Delta E$  strip, the solid angles  $\Delta\Omega_{s,\theta}$  covered by any polar angle  $\theta$  inside any  $\Delta E$  strip and the detector solid angles  $\Delta\Omega_\theta$  covered by any polar angle  $\theta$ . In this way it is possible to reconstruct the  $^{17}\text{F}$  scattering angular distribution in the laboratory frame directly from the counts of each strip ( $n_s$ ), using the formula:

$$\frac{d\sigma}{d\Omega}(\theta) = \frac{\sum_s n_s \left( \frac{\Delta\Omega_{s,\theta}}{\Delta\Omega_s} \right)}{\Delta\Omega_\theta} \times \frac{\sum_{\theta_F} \left( \frac{d\sigma_R}{d\Omega}(\theta_F) \right) \Delta\Omega_{\theta_F}}{n_F} \quad (1)$$

In the first factor we added the strip count numbers

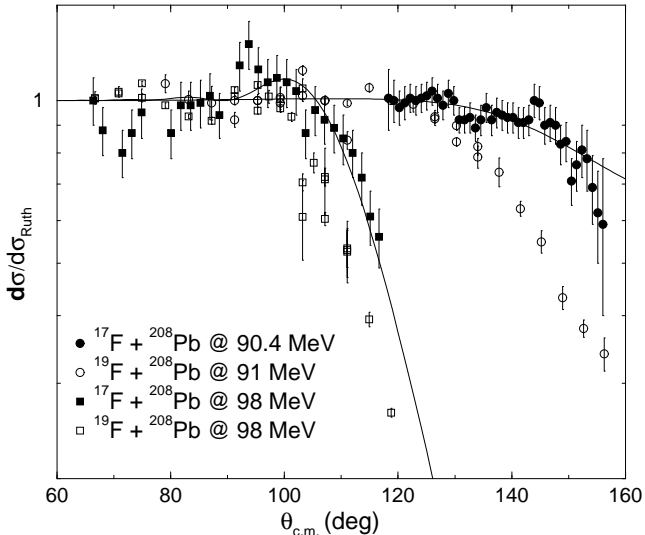


FIG. 5:  $^{17}\text{F}(^{19}\text{F}) + ^{208}\text{Pb}$  quasi elastic scattering angular distributions at 90.4(91) and 98 MeV beam energy. The continuous lines are the results of the optical model best fits for the  $^{17}\text{F}$  system. The parameters used at 90.4 MeV for the system  $^{17}\text{F} + ^{208}\text{Pb}$  are listed in table II, while for the data at 98 MeV we used the same sets, but the imaginary depth ( $W_0 = 12.8$  MeV), in order to minimize the  $\chi^2$ . The quoted errors for the data at 90.4 MeV are statistical, whereas those at 98 MeV include both statistical and systematical uncertainty.

$n_s$ , weighted by the ratio  $\frac{\Delta\Omega_{s\theta}}{\Delta\Omega_s}$ , over all the strips  $s$  containing the polar angle  $\theta$ . The second ratio is the normalization factor, obtained by adding the Rutherford cross section  $\frac{d\sigma_R(\theta_F)}{d\Omega}$  at forward angles  $\theta_F$ , weighted by the detector solid angle  $\Delta\Omega_{\theta_F}$  subtended by each polar angle  $\theta_F$ , and dividing by the total number  $n_F$  of events collected in the  $\Delta E$  forward detector. The uncertainty in solid angle Monte-Carlo calculations was estimated to be smaller than 1%.

Fig. 5 presents the evaluated  $^{17}\text{F}$  scattering differential cross section, after geometrical correction. Because of the target thickness and the target frame screening, only the experimental points above  $115^\circ$  could be evaluated; only the statistical errors have been plotted in the figure. The differential cross section is flat up to  $\sim 130^\circ$  followed by a slight decrease.

For comparison, in the same figure, we have also included the elastic scattering angular distributions measured for the same system at 98 MeV (taken from [12]) and for the system  $^{19}\text{F} + ^{208}\text{Pb}$  at 91 and 98 MeV beam energy [13].

## 2. Breakup event analysis

We have also performed an exclusive analysis to search for breakup events  $^{17}\text{F} \rightarrow ^{16}\text{O} + p$  ( $S_p = 0.601$  MeV). In this reaction channel the  $^{16}\text{O}$  stops in the  $\Delta E$  layer while the proton stops in the E layer. This is the case where

the capabilities of EXODET telescope are particularly important. We have imposed the following conditions: a) two strips of the  $\Delta E$  detector and only one of the E should be hit; b) the JT of all the strips should be in the correlation peak; c) the ToT of one strip of the  $\Delta E$  should be in the Fluorine-Oxygen range while the ToT of the other should be lower; d) the total energy released in the  $\Delta E$  detector should be, for kinematics reasons, in the spectrum region of the  $^{17}\text{F}$  and  $^{17}\text{O}$  elastic peaks (total energy of  $^{16}\text{O}$  added to the proton energy lost).

From kinematical calculations the relative angle between the proton and the  $^{16}\text{O}$  velocity vectors has a maximum value of  $25^\circ$  at 1 MeV  $^{17}\text{F}$  excitation energy above the breakup threshold. Therefore, one single telescope has enough solid angle to cover the whole kinematical range. Monte-Carlo simulation confirm that the efficiency of the EXODET apparatus for the detection of the  $^{17}\text{F}$  breakup events is above 90% up to 1.25 MeV excitation energy above the threshold. To extract the cross section we have evaluated the detection efficiency of protons and  $^{16}\text{O}$  ions (intrinsic efficiency) and we have estimated the solid angle coverage of each strip by a Monte-Carlo simulation (geometrical efficiency). The cross section is obtained by normalizing the obtained yield to the Rutherford cross section. The error takes into account both the statistical error and the uncertainties in the above efficiencies. The differential cross section deduced for the breakup process  $^{17}\text{F} \rightarrow ^{16}\text{O} + p$  has an average value of  $2.6 \pm 1.2$  mb/sr.

## IV. THEORETICAL ANALYSIS AND DISCUSSION

### A. Optical Model analysis

The experimental data were fitted in the framework of the optical model using the fitting subroutines of the code FRESKO [14]. The aims of the analysis are manifold: (i) to investigate the influence of the low binding energy onto the potential, (ii) to get consistent optical model parameter sets, (iii) to define the potential around the strong absorption radius and (iv) to compare these results with those obtained for similar mass systems, particularly with those involving stable well-bound isotopes.

It is known that in this energy range the analysis of complex ion elastic scattering will lead to non unique sets of parameters. However the potential values at the strong absorption radius are usually well defined and rather independent from all the fitting ambiguities. This corresponds to a surface interaction of the colliding nuclei.

In this paper we followed the procedure adopted in [13] for the  $^{19}\text{F} + ^{208}\text{Pb}$  reaction. We chose a Woods-Saxon well for the real and the imaginary potential, fixing the radii ( $r_{0v} = r_{0w} = r_0$ ) and the diffusenesses ( $a_v = a_w = a_0$ ) and varying the depths ( $V_0$  and  $W_0$ ). In order to check the influence of each potential parameter, we performed different fits. We selected two grids: one with

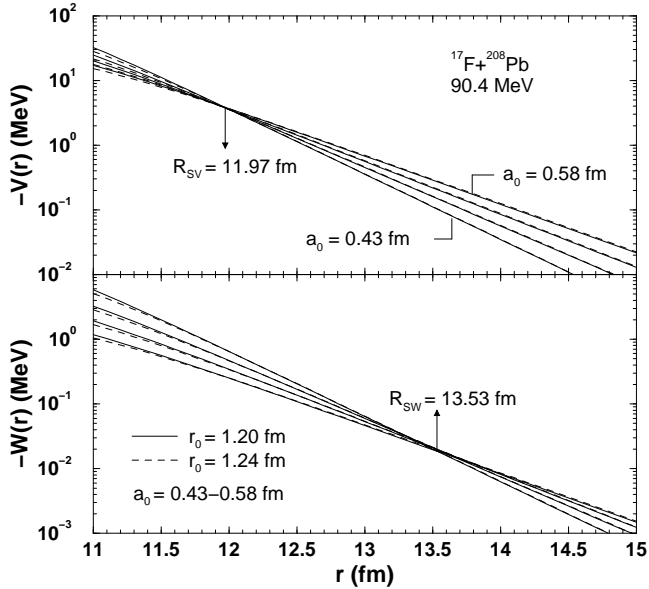


FIG. 6: Behaviour of real and imaginary potential fitting the  $^{17}\text{F}$  elastic scattering data at 90.4 MeV for the different values of diffuseness and radius listed in Table I.

TABLE I: Upper (lower) panel: optical model parameters obtained from the best fits of the  $^{17}\text{F}$  elastic scattering data, fixing  $r_0 = 1.20$  (1.24) fm and varying the diffuseness.

$r_0 = 1.20$ fm			
$a_0$ (fm)	$V_0$ (MeV)	$W_0$ (MeV)	$\chi^2/pt$
0.43	$242.3 \pm 41.6$	$43.6 \pm 14.8$	0.509
0.48	$156.1 \pm 22.4$	$20.6 \pm 6.8$	0.506
0.53	$111.6 \pm 13.1$	$10.7 \pm 3.4$	0.503
0.58	$86.0 \pm 8.4$	$5.9 \pm 1.9$	0.500
$r_0 = 1.24$ fm			
$a_0$ (fm)	$V_0$ (MeV)	$W_0$ (MeV)	$\chi^2/pt$
0.43	$111.1 \pm 18.8$	$20.1 \pm 6.7$	0.508
0.48	$78.4 \pm 10.6$	$10.3 \pm 3.2$	0.505
0.53	$60.5 \pm 6.2$	$5.7 \pm 1.8$	0.501
0.58	$49.3 \pm 2.5$	$3.4 \pm 0.8$	0.496

a fixed radius parameter ( $r_0 = 1.20$  and 1.24 fm) and the other with four values for the diffuseness parameter ( $a_0 = 0.43, 0.48, 0.53$  and 0.58 fm). For each set we calculated the best  $V_0$  and  $W_0$  minimizing the  $\chi^2$ . Table I summarizes the results of the analysis and Fig. 6 shows the behaviour of both real and imaginary part of the potential near the strong absorption radii.

The fits were performed assuming that the collected data originated only from pure elastic scattering, since, as already mentioned, our energy resolution did not allow to solve possible excitations to the only  $^{17}\text{F}$  excited state below the breakup threshold ( $E_x = 0.4953$  MeV) and to the first  $^{208}\text{Pb}$  excited level ( $E_x = 2.614$  MeV). We verified our assumption *a posteriori*, running FRESKO within the DWBA approach, using the potential parameters obtained from the previous best-fit analysis and including

the possibility to excite the first  $^{17}\text{F}$  excited state, with the experimental transition probability  $B(E2)_{\uparrow} = 21.64$   $\text{e}^2\text{fm}^4$  [15]. It was seen that, in this energy range, the contribution of this channel to the quasi-elastic cross section was at maximum  $\sim 2\%$  and for this reason, it could be neglected in first approximation. We also checked the possible excitation to the first  $^{208}\text{Pb}$  excited state ( $3^-, E_x = 2.614$  MeV) and saw that this contribution was lower than 1% at all angles with respect to the quasi-elastic cross section.

## B. Strong absorption radii

From the performed analysis, both real and imaginary strong absorption radii were deduced:  $R_{SV} = 11.97 \pm 0.14$  fm and  $R_{SW} = 13.53 \pm 0.19$  fm. The potentials at these points are  $V_{sa} = 3.84 \pm 0.51$  MeV and  $W_{sa} = 0.020 \pm 0.002$  MeV, respectively. These values are quite different from each other with the imaginary part of the potential well outside the nucleus core. This scenario is completely different for the stable isotope  $^{19}\text{F}$ . In fact for the system  $^{19}\text{F} + ^{208}\text{Pb}$  at 91 MeV beam energy, the real and imaginary strong absorption radii, reported in [13] are very similar ( $R_{SV} = 12.32$  fm and  $R_{SW} = 12.12$  fm).

Within the same framework we have also fitted the elastic scattering data for the  $^{17}\text{F} + ^{208}\text{Pb}$  reaction at 98 MeV beam energy. In this case we adopted two procedures, with the same  $r_0$  and  $a_0$  grids used previously: a) we fixed the real part of the potential at the value obtained from our previous data analysis at 90.4 MeV beam energy and varied only  $W_0$  in order to minimize the  $\chi^2$ ; b) we varied both  $V_0$  and  $W_0$ , using the previously calculated values as starting points.

The two procedures gave slightly different results, but leading to the same conclusions. From the first approach, we could estimate an imaginary strong absorption radius  $R_{SW} = 13.08 \pm 0.03$  fm and the corresponding potential  $W_{sa} = 0.102 \pm 0.007$  MeV. From the second analysis, we obtained  $R_{SV} = 12.20 \pm 0.08$  fm for the real part and  $R_{SW} = 12.67 \pm 0.18$  fm for the imaginary part. The values of the two potentials at these points were  $V_{sa} = 2.23 \pm 0.09$  MeV and  $W_{sa} = 0.27 \pm 0.03$  MeV, respectively.

We can compare these radii with the ones obtained for the system  $^{19}\text{F} + ^{208}\text{Pb}$  at 98 MeV beam energy:  $R_{SV} = 12.62$  fm and  $R_{SW} = 12.75$  fm [13]. Also at this energy the  $^{17}\text{F}$  imaginary (absorptive) potential extends well outside the core, which is not the case for  $^{19}\text{F}$  ( $R_{SV} \sim R_{SW}$ ). This effect might be caused by the low binding energy of the last proton in  $^{17}\text{F}$ .

## C. Reaction cross sections

In Fig. 7 we compare our elastic scattering angular distributions with the optical model analysis of the experimental data for four systems:  $^{16}\text{O} + ^{208}\text{Pb}$  ( $S_p = 12.127$  MeV) [16],  $^{17}\text{O} + ^{208}\text{Pb}$  ( $S_n = 4.143$  MeV) [17]

TABLE II: Optical model potential parameters obtained from the best fit of four different reactions. The data for fluorine isotopes arise from our analysis, while the data for oxygen isotopes are taken from [16] and [17], respectively.

reaction	$E_{lab}$ (MeV)	$E_{cm}/V_c$	$V_0$ (MeV)	$r_{0v}$ (fm)	$a_v$ (fm)	$W_0$ (MeV)	$r_{0w}$ (fm)	$a_w$ (fm)	$\chi^2/pt$	$\sigma_R$ (mb)
$^{17}\text{F} + ^{208}\text{Pb}$	90.4	0.96	$60.5 \pm 6.2$	1.24	0.53	$5.7 \pm 1.8$	1.24	0.53	0.501	77
$^{19}\text{F} + ^{208}\text{Pb}$	91	0.96	$107.6 \pm 6.1$	1.24	0.53	$20.1 \pm 3.0$	1.24	0.53	1.111	269
$^{16}\text{O} + ^{208}\text{Pb}$	78	0.93	78.28	1.215	0.65	17.11	1.162	0.623	0.99	47
$^{17}\text{O} + ^{208}\text{Pb}$	78	0.93	82.81	1.226	0.65	9.93	1.226	0.60	1.25	91

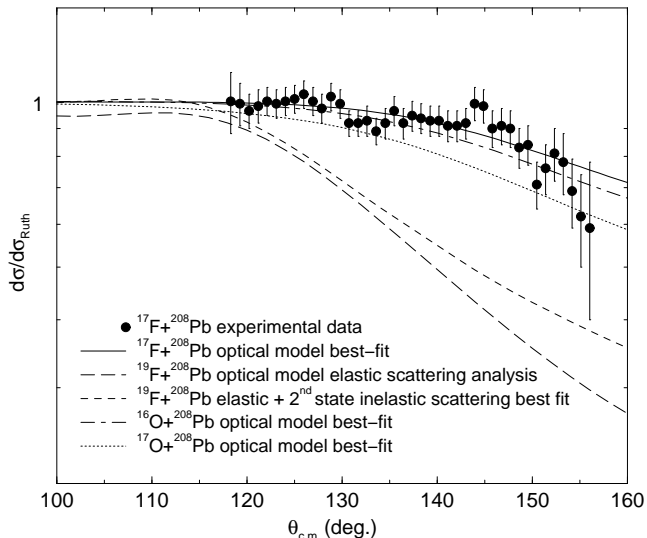


FIG. 7: Comparison of the optical model analysis of the experimental elastic scattering angular distributions for 4 different systems:  $^{16,17}\text{O} + ^{208}\text{Pb}$  at 78 MeV,  $^{17}\text{F} + ^{208}\text{Pb}$  at 90.4 MeV and  $^{19}\text{F} + ^{208}\text{Pb}$  at 91 MeV beam energy. The potential parameters used are indicated in Table II. For the reaction involving  $^{19}\text{F}$ , we adopted the standard Woods-Saxon already used for  $^{17}\text{F}$ , adding the excitation to the second excited state at  $E_x = 0.197$  MeV from a DWBA calculation (the first level at  $E_x = 0.110$  MeV was not included, since its coupling to the ground state is very weak). The curve labelled “elastic + 2<sup>nd</sup> state inelastic scattering best fit” is the result of this calculation. From this analysis, it was also possible to extract the pure elastic data (the curve labelled “optical model elastic scattering analysis”). Experimental data for the  $^{17}\text{F} + ^{208}\text{Pb}$  system studied in this paper are also shown for completeness.

at 78 MeV,  $^{17}\text{F} + ^{208}\text{Pb}$  ( $S_p = 0.601$  MeV) at 90.4 MeV and  $^{19}\text{F} + ^{208}\text{Pb}$  ( $S_p = 7.994$  MeV) [13] at 91 MeV beam energy. At these energies, the ratios  $E_{cm}/V_c$  are very similar for all the systems, as reported in Table II. We clearly see that the  $^{17}\text{F}$  cross section is much more similar to that of the Oxygen isotopes rather than to both the elastic and quasi-elastic  $^{19}\text{F}$  cross sections. This fact was quite surprising, since the radioactive and very weakly bound  $^{17}\text{F}$  was expected to behave differently from the well-bound  $^{16}\text{O}$  and  $^{17}\text{O}$ .

Table II summarizes the parameters used to fit the four systems and in the last column we also list the values of the deduced reaction cross sections. The  $^{19}\text{F}$  data

were reanalyzed using the same procedure as for  $^{17}\text{F}$  and the results are slightly different with respect to the published data [13]; Table II reports the values obtained from our analysis. The reaction cross sections for the  $^{16,17}\text{O}$  and  $^{17}\text{F}$  projectiles are similar and they are quite smaller (about a factor 3) in comparison to the  $^{19}\text{F}$  case. This large difference could originate from the collective structure of  $^{19}\text{F}$ , since its ground state ( $J^\pi = \frac{1}{2}^+$ ) is very strongly coupled to the excited state at  $E_x = 0.197$  MeV, ( $J^\pi = \frac{5}{2}^+$ ), belonging to the same rotational band [18]. To check this point, we have performed DWBA calculations for the excitations to this (collective) excited state in  $^{19}\text{F}$  as well as to the  $^{17}\text{F}$  first (single-particle) excited level. For  $^{19}\text{F}$  ( $^{17}\text{F}$ ), the contribution of the calculated inelastic scattering cross section to the elastic scattering angular distribution is fairly large (small) [ $\sim 20\%$  ( $2\%$ )]. Therefore, we can conclude that at Coulomb barrier energies, it seems to be easier to excite collective structures (even in a well-bound nucleus like  $^{19}\text{F}$ ) than to breakup a very loosely-bound nucleus, as  $^{17}\text{F}$ . We have to bear in mind that in the  $^{19}\text{F}$  case the low excitation energy as well as the strong transition probability  $B(E2)$  enhances this process.

#### D. Breakup cross section

The average value for the differential cross section of the breakup process  $^{17}\text{F} \rightarrow ^{16}\text{O} + p$  is  $2.6 \pm 1.2$  mb/sr. The cross section of the “two-body” breakup process (with both  $^{16}\text{O}$  and  $p$  in the exit channel) is rather small, if the behaviour at forward angles is the same as at backward angles. Similar results for this system have already been observed at 170 MeV bombarding energy, well above the Coulomb barrier, where the cross section for the “two-body” breakup [19] was found to be much smaller than the “one-body” breakup [20] (only  $^{16}\text{O}$  in the exit channel). These results are in good agreement with the predictions of Esbensen [21].

Therefore, we can conclude that at energies around the Coulomb barrier the “one-body” breakup is the strongest breakup process. A similar result has already been observed for the system  $^6\text{Li} + ^{208}\text{Pb}$  at Coulomb barrier energies: the cross section of the one-body (inclusive) breakup was found to be  $\sim 5$  times larger than that of the two-body (exclusive) breakup [7, 22].

## V. CONCLUSIONS

In the present paper the  $^{17}\text{F}$  scattering from a  $^{208}\text{Pb}$  target has been studied at energies around the Coulomb barrier with the large solid angle detector array EX-ODET.

The  $^{17}\text{F}$  angular distribution was measured in the polar angle  $\theta$  range from  $115^\circ$  to  $155^\circ$  and an optical model analysis was performed in order to get the best fit potential parameters. The values of the real and imaginary strong absorption radii were calculated and both potentials at these radial points determined. The results at 90.4 and 98 MeV were compared with those obtained for the system  $^{19}\text{F} + ^{208}\text{Pb}$  at about the same  $E_{cm}/V_c$  values. Contrary to  $^{19}\text{F}$ , the strong absorption radii of the imaginary potential are systematically  $\sim 10\%$  larger than those of the real potential. This effect might be due to

the very small  $^{17}\text{F}$  binding energy.

The elastic scattering angular distributions of these two isotopes are quite different; the  $^{17}\text{F}$  cross sections are very similar to those of the well-bound nuclei  $^{16,17}\text{O}$ , while the  $^{19}\text{F}$  reaction cross section turns out to be a factor 3 larger. From this observation we conclude that in our case collective modes in  $^{19}\text{F}$  are stronger than the breakup probability in  $^{17}\text{F}$ .

We have also performed a first direct measurement of the breakup process  $^{17}\text{F} \rightarrow ^{16}\text{O} + p$  cross section below the Coulomb barrier. The rather small cross section value is not in contradiction to the large breakup probability, under the hypothesis that the strongest breakup channel has only one outgoing fragment ( $^{16}\text{O}$ ), while the other fragment ( $p$ ) is captured by the target. This behaviour is in agreement with what found in the system  $^6\text{Li} + ^{208}\text{Pb}$  [22].

- 
- [1] M. A. Nagarajan, J. Phys. G **23**, 1479 (1997).
  - [2] E. F. Aguilera *et al.*, Phys. Rev. Lett. **84**, 5058 (2000).
  - [3] C. Signorini *et al.*, Phys. Rev. C **61**, 061603(R) (2000).
  - [4] N. Keeley *et al.*, Nucl. Phys. **A571**, 326 (1994).
  - [5] G.R. Kelly *et al.*, Phys. Rev. C **63**, (2000) 024601.
  - [6] C. Signorini *et al.*, *Nucleus-Nucleus Collisions*, Proceedings of the International Conference *BO2000*, Bologna, Italy, May 2000, edited by G.C. Bonsignori *et al.*, (World Scientific, Singapore 2001) p.413.
  - [7] C. Signorini *et al.*, Phys. Rev. C **67**, 044607 (2003).
  - [8] R. Marlock *et al.*, Phys. Rev. Lett. **79**, 3837 (1997).
  - [9] M. J. Borge *et al.*, Phys. Lett. **B217** 25 (1993).
  - [10] B. Harss *et al.*, Rev. Sci. Instrum. **71**, 380 (2000).
  - [11] A. Parazzo *et al.*, BABAR Note #501 (1999).
  - [12] J. F. Liang *et al.*, Phys. Rev. C **67**, 044603 (2003).
  - [13] C. J. Lin *et al.*, Phys. Rev. C **63**, 064606 (2001).
  - [14] I. J. Thompson, Comput. Phys. Rep. **2**, 167 (1998).
  - [15] D. R. Tilley *et al.*, Nucl. Phys. **A565**, 1 (1993).
  - [16] I. J. Thompson *et al.*, Nucl. Phys. **A505**, 84 (1989).
  - [17] J. S. Lilley *et al.*, Nucl. Phys. **A463**, 710 (1987).
  - [18] D. R. Tilley *et al.*, Nucl. Phys. **A595**, 1 (1995).
  - [19] J. F. Liang *et al.*, Phys. Lett. **B491** 23 (2000).
  - [20] J. F. Liang *et al.*, Phys. Rev. C **65**, 051603 (2002).
  - [21] K. E. Rehm *et al.*, Phys. Rev. Lett. **81**, 3341 (1998).
  - [22] C. Signorini *et al.*, Proceedings of the International Conference Fusion03, Matsushima, Miyagi, Japan, Nov 2003, eds. N. Takigawa *et al.* to be published in Progress of Theoretical Physics.